CHEMISTRY
A EUROPEAN JOURNAL

DOI: 10.1002/chem.200600463

From Supramolecular Porphyrin Tweezers to Dynamic $A_nB_mC_lD_k$ Multiporphyrin Arrangements Through Orthogonal Coordination

Ravuri S. K. Kishore, Thomas Paululat, and Michael Schmittel*[a]

Abstract: A dynamic, supramolecular, three-component $A_nB_mC_l$ bis(zinc porphyrin) tweezer has been prepared quantitatively using the heteroleptic bisphenanthroline (HETPHEN) concept. Upon addition of nitrogenous spacers of different length, namely, the extended bipyridine **3a**, 4,4′-bipyridine (**3b**), and 1,4-diazabicyclo[2.2.2]octane (DABCO; **3c**), to set up an additional orthogonal binding motif (Zn_{Por}–N_{spacer}), three structurally different, still dynamic, four-component $A_nB_mC_lD_k$ assemblies were cleanly formed, as indicated by UV/Vis and NMR titrations as well as by DOSY investigations. The structures were identified as a bridged monotweezer A_2BC_2D, a doubly bridged double tweezer $A_4B_2C_4D_2$, and a triply bridged double tweezer $A_4B_2C_4D_3$, the latter resembling a porphyrin stack. Notably, the same structures were equally formed directly from a mixture of the constituents A, B, C, and D put together in any sequence if the correct stoichiometry was applied.

Keywords: N ligands · nanostructures · porphyrinoids · self-assembly · supramolecular chemistry

Introduction

The ultimate goal of supramolecular science is to attain a level of complexity and sophistication in structure and function similar to that commonly observed in natural supramolecular assemblies.[1] Nature adopts an omnifarious strategy for the creation of tertiary supramolecular structures from simple molecules by exploiting a combination of noncovalent and weak interactions in a reversible and thermodynamically controlled process, to finally achieve the required topology along with an appreciable conformational rigidity for high-end physiological functions. A major factor responsible for such exceptional organization in natural systems is the use of modular and hierarchical self-assembly. The molecular information necessary for self-assembly is designated to and disseminated over multiple levels of organization, which results in a structural and functional hierarchy that delivers a high-fidelity output at each level of organization and as a whole unit. An ideal mimic of the natural process would therefore require the self-assembly of various components, each supplying an input through specific molecular information and orthogonal binding modes, which under equilibrium conditions would develop into one single aggregate.

Over the past two decades there have been zealous attempts to fabricate intricate supramolecular structures by utilizing diverse intermolecular interactions and multiple molecular components.[2] At present, higher-order, nanoscale supramolecular structures are forged by the use of multiples of up to three components and a single binding algorithm (A_nB_m or $A_nB_mC_l$),[1,2] while, surprisingly, very few examples are known with four or more molecular components ($A_nB_mC_lD_k$).[3] Hence, in spite of some fascinating examples of supramolecular assemblies by Lehn, Fujita, Stang, Reinhoudt, and many others,[4] the design and preparation of higher-order aggregates with four or more different components[5] (i.e., modular building blocks) using orthogonal complexation motifs[6] still remain a challenge. The clear solution lies in choosing compatible assembly modules that are co-existent in the final assembly. The present study is an endeavor in this direction.

Starting from our ongoing work directed toward heteroleptic nanoscale architectures,[7] we decided to elaborate the three-component self-assembly into a four-component one utilizing noninterfering orthogonal binding algorithms under thermodynamic equilibration conditions (Figure 1). The Cu^I heteroleptic bisphenanthroline (HETPHEN) complexation

[a] R. S. K. Kishore, Dr. T. Paululat, Prof. Dr. M. Schmittel
Center of Micro- and Nanochemistry and Engineering
Organische Chemie, Universität Siegen
Adolf-Reichwein-Strasse, 57068 Siegen (Germany)
Fax: (+49) 271-740-3270
E-mail: schmittel@chemie.uni-siegen.de

Supporting information (experimental procedures, ^1H NMR spectra, ESI-MS data, Jobs plot analyses, and DOSY plots) for this article is available on the WWW under http://www.chemeurj.org/ or from the author.

motif[8] was thus supplemented by the Zn_{Por}–N_{spacer} (zinc porphyrin–DABCO/bipyridyl; DABCO = 1,4-diazabicyclo-[2.2.2]octane) interaction, a motif that has been used earlier to assemble cofacial higher-order porphyrin structures[9] and to study the dynamics therein.[10] Interest in such systems arises from the fact that successful light harvesting occurs solely by congruous arrangement of constituent porphyrins and appropriate cofacial stacking.[11] Moreover, cofacial porphyrin arrangements have raised vast interest due to their suitability for controlled electrochemical processes, such as the four-electron reduction of dioxygen to water.[12] Although considerable research has gone into the generation of highly preorganized, cofacially arranged bis-porphyrins, almost all studies concern a covalently designed framework.[9,10] The present work not only describes for the first time the preparation of supramolecular tweezers, but also demonstrates how the tertiary structure of a supramolecular arrangement can be drastically modified as a function of the length of an orthogonally operating building block.

Results and Discussion

The components used in this study include the phenanthroline-appended porphyrin **1**, the linear bisphenanthroline **2**, the spacers **3a–c** [1,4-bis(4′-pyridylethynyl)durene (**3a**; d_{NN} = 16 Å), 4,4′-bipyridine (**3b**; d_{NN} = 7 Å), and DABCO (**3c**; d_{NN} = 3 Å)], and $[Cu(CH_3CN)_4]PF_6$ as the coordinating metal salt. The phenanthroline–porphyrin hybrid **1** and bisphenanthroline **2** were synthesized by Sonogashira coupling reactions based on earlier reports.[7d,13] Equally, **3a** was prepared in 68% yield by a Sonogashira coupling based on an analogous compound [Eq. (1)].[14]

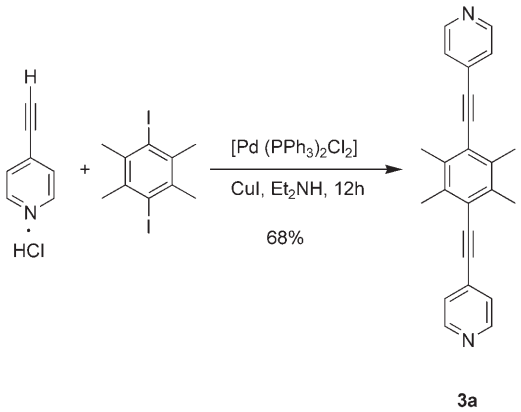

(1)

Preparation of porphyrin tweezer PT by a three-component assembly: As a result of the HETPHEN algorithm[8] implanted into the ligands, quantitative heteroleptic complexation of ligand **1** in the presence of $[Cu(CH_3CN)_4]PF_6$ with 1,10-phenanthroline (**5**) and bisphenanthroline **2** was observed, which afforded **4** and the supramolecular porphyrin tweezer **PT**, respectively, as exclusive products (Scheme 1). The formation of **PT** is reminiscent of the formation of other supramolecular racks whose structure (by X-ray diffraction) and dynamics have been investigated extensively.[7f]

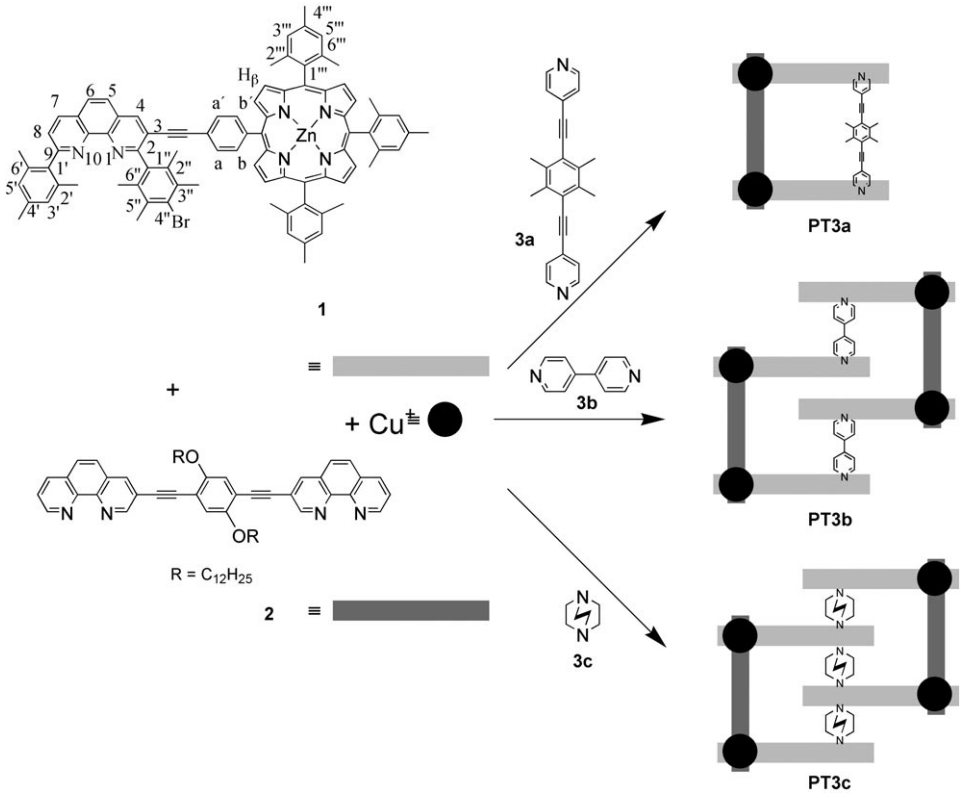

Figure 1. A four-component self-assembly process that is controlled by the length of the linear ligand **3**.

Complexes **4** and **PT** were characterized by ESI-MS, and gave signals of 100% intensity at *m*/*z* 1580 and 1825 (dication), respectively. The isotopic splitting patterns obtained in ESI-MS fitted accurately with the simulated splitting patterns (Figure S4 in Supporting Information). Moreover, the ^{1}H NMR spectra displayed a characteristic upfield shift of the 3′,5′-mesitylene protons (3′,5′-MesH) of **1** due to shielding from the second phenanthroline π system (**5** or **2**).

The ^{1}H NMR spectrum of complex **4** shows a single signal for the enantiotopic 3′,5′-MesH due to the plane of symmetry along the phenanthroline–≡–

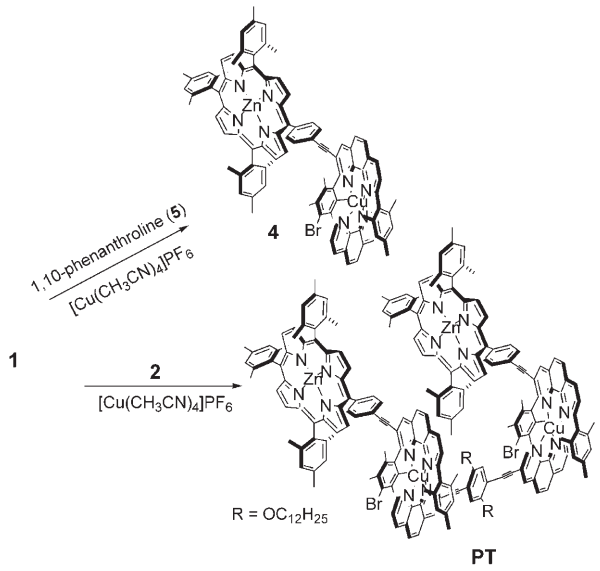

Scheme 1. Synthesis of **4** and the supramolecular porphyrin tweezer **PT**.

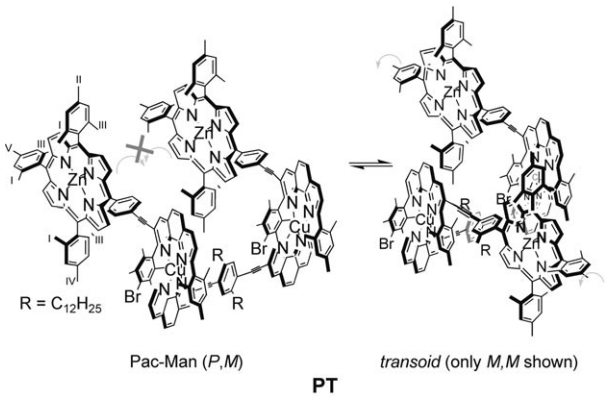

Scheme 2. Dynamic equilibration of **PT** by dissociation/association and bond rotation. The roman numerals represent the assignment to the five sets of Mes-CH_3 protons which appear in the ^{1}H NMR spectrum of **PT**.

porphyrin axis. In contrast, the porphyrin assembly **PT** exhibits two sets of diastereotopic protons due to the nonequivalence of the 3′,5′-MesH (Figure 2), since the plane of symmetry has disappeared. Similarly, Mes-CH_3 protons of the porphyrin (2‴,4‴,6‴-CH_3) in **4** at $\delta \approx 1.83$–1.86 ppm appear only as two singlets (Figure S5 in Supporting Information), while the corresponding Mes-CH_3 protons in **PT** show up as five sets (Figure S6 in Supporting Information) assignable to a set of rapidly equilibrating configurations (*meso* and *P,P*/*M,M*) as shown in Scheme 2. Due to the dynamic nature of its Cu^I metal ion–ligand interaction, **PT** cannot be isolated or differentiated by ^{1}H NMR spectroscopy. In addition, various conformations (*cisoid* = Pac-Man and *transoid*) may arise because of rotation about the bisphenanthroline axis.

Although the porphyrin units should be free to rotate perpendicularly to the bisphenanthroline backbone, free rotation is only possible in the *transoid* conformation. In the *cisoid* conformation, the simultaneous rotation of the two

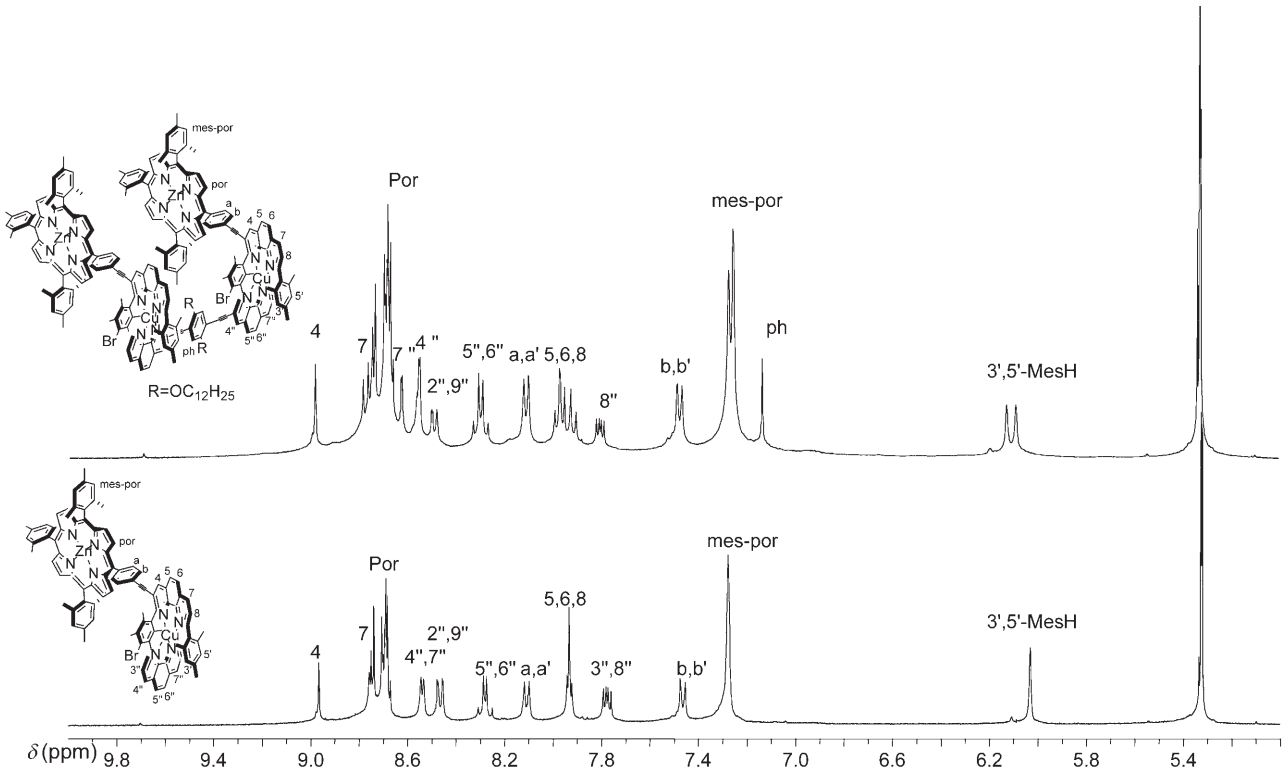

Figure 2. Comparison of the aromatic region in the NMR spectra of **PT** (top) and **4** (bottom).

porphyrins of **PT** is prohibited due to hindrance caused by the mesityl groups, thus confining *cisoid*-**PT** to a tweezer-like conformation with cofacial porphyrins as shown in Scheme 2 (left).

Four-component assemblies: The porphyrin tweezer **PT** displays a "Pac-Man"-like arrangement in its *cisoid* (*P*,*M*) configuration exhibiting a distance of 19 Å between the cofacial porphyrins, as evaluated from the PM3 optimized model.[15] Most known Pac-Man porphyrins[11] require an optimum distance of 7 Å[9a,b] for a single "bite" complexation to a DABCO molecule. In the case of larger inter-porphyrin distances, as in **PT**, clearly a longer bis-nitrogen ligand is needed to achieve a 1:1 **PT**·(bidentate base) host–guest aggregate.[16]

After the initial construction of a 1:1 assembly of **PT** and **3a** ($d_{NN}=16$ Å), it was decided to shorten the N···N distance of the bis-nitrogen ligand by using **3b** ($d_{NN}=7$ Å) and **3c** ($d_{NN}=3$ Å) and to investigate the nature of the assemblies formed by UV and NMR spectroscopy. Upon addition of **3a–c** to **PT** distinct changes were noticed in the spectra, as summarized in Table 1. A Jobs plot analysis revealed an optimum 1:1 stoichiometry for **PT·3a** and **PT·3b**, but a reproducible ratio of 1:1.5 was obtained for **PT·3c** (Figure S17 in Supporting Information).

Table 1. Data from UV/Vis and NMR spectroscopy investigations (for numbering, see Figure 1).

	Jobs plot analysis[a]	Soret band abs [nm][a]	δ of H_β [ppm][b]	δ of porphyrin Mes-CH_3 [ppm][b]	δ of 3′,5′-MesH [ppm][b]
PT		420	8.69–8.78 (m)	1.17–1.92 (m)	6.12 (s), 6.16(s)
PT·3a	1:1	430	8.64–8.70 (m)	1.79 (s), 1.81(s), 1.82 (s)	6.12 (s)
PT·3b	1:1	425 (1:1), 430 (1:2)	8.50–8.63 (m)	1.56–1.60 (m)	6.05 (s), 6.06 (s), 6.16 (s), 6.19 (s)
PT·3c	1:1.5	425 (1:1.5), 430 (1:2)	8.28–8.35 (m)[c]	1.43–1.51 (m)	6.06 (s), 6.09 (s), 6.21 (s), 6.23 (s)[c]

[a] Measured in CH_2Cl_2 at 25 °C. [b] Measured in CD_2Cl_2. [c] NMR measured at a **PT·3c** ratio of 1:1.5.

NMR analysis: In all adducts at ideal stoichiometry (based on the Jobs plot analysis), that is, **PT·3a,b** (1:1) and **PT·3c** (1:1.5), the porphyrin H_β signals exhibited significant upfield shifts due to axial coordination of ligand **3**, the degree varying with the binding affinity.[9,10] While the upfield shift was $\Delta\delta(H_\beta)=0.05$ ppm for **PT·3a** versus **PT**, $\Delta\delta(H_\beta)$ was increased to 0.2 ppm for **PT·3b** and to 0.4 ppm for **PT·3c**. In the same manner, the 3‴,5‴ mesitylene protons ($\delta=7.0$–7.5 ppm) at the porphyrin (PorMes-*H*) were found to shift upfield increasingly in the series **PT** < **PT·3a** < **PT·3b** ≈ **PT·3c** (Figure 3). The signal pattern of the 3′,5′-Mes-H protons at $\delta=6.2$ ppm served as a diagnostic tool for the symmetry of the molecule and provided insight into the possible structure. Thus, while a single signal was observed for **4**, two singlets were noticed in **PT** due to a breakdown in symmetry. Similarly, one singlet was noticed with **PT·3a**, while four singlets were observed for **PT·3b,c**. Notably, a distinct similarity of the various shifts was noticed in the ^{1}H NMR spectrum of **PT·3b** (1:1) and **PT·3c** (1:1.5). It could thus be speculated that a similar structural composition is achieved in both the complexes.

Further evidence for the formation of the adducts was derived from the significant ^{1}H NMR shifts of the diaza spacers **3a–c**. In the case of **PT·3a**, the 3,3′ protons of **3a** at $\delta=8.61$ ppm shifted upfield to 6.50 and 6.70 ppm (Figure 3), as is known for related complexes.[9a,b] Additionally, the signal of the CH_3 protons of **3a** shifted upfield from $\delta=2.50$ to 2.10 ppm. In **PT·3b**, the signals of the 2,2′ protons of **3b** shifted upfield to $\delta=2.32$ ppm, while those of the 3,3′ protons were observed at $\delta=4.96$ ppm.

The addition of 1.5 equivalents of DABCO (**3c**) to **PT** (based on the stoichiometry obtained from the Jobs plot) produced substantial changes which were monitored by NMR and UV spectroscopy. ^{1}H NMR titration of **PT** with **3c** at the millimolar concentration level provided particular insight. Upon addition of one equivalent of **3c**, two signals at $\delta=$

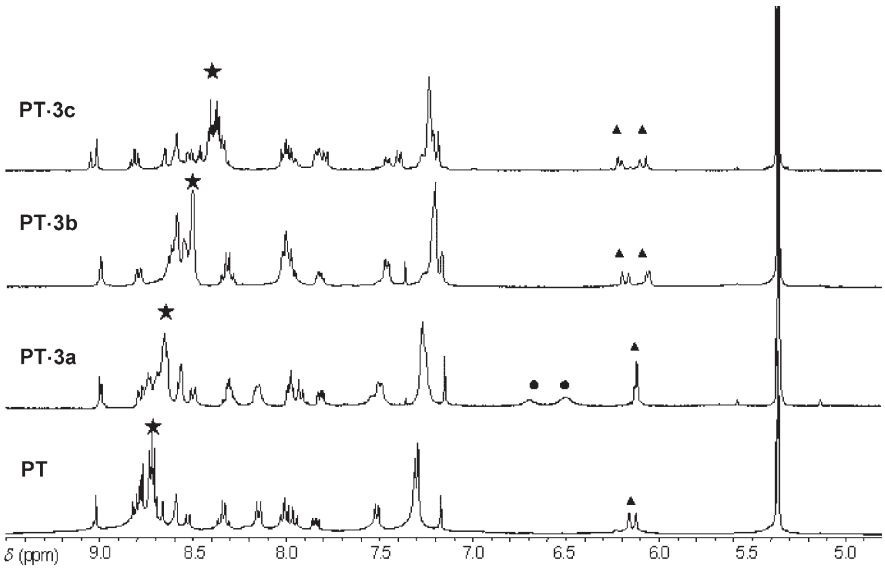

Figure 3. Comparison of **PT** with **PT·3a**, **PT·3b** (1:1 composition), and **PT·3c** (1:1.5 composition). (*) Porphyrin H_β signals in **PT·3a–c**; (▲) protons corresponding to 3′,5′-MesH; (●) upfield-shifted 3,3′-pyridyl protons of **3a**.

−4.5 and −4.7 ppm emerged in the ^{1}H NMR spectrum. As a sharp singlet in this region is unequivocal proof for the formation of a porphyrin–**3c** (2:1) complex,[9,10] the presence of two signals indicates two distinct environments of the DABCO methylene protons. The signal at $\delta = -4.5$ ppm appeared as a sharp singlet from the very first few aliquots added, whereas the latter developed gradually and gained equal integrated peak area and intensity during addition until a 1:1 mole ratio of DABCO to **PT** was reached. As a COSY spectrum of **PT·3c** (1:1) revealed no cross-peaks between the two signals, we concluded that two distinct DABCO–porphyrin sandwich complexes were present in the assembly. The formation of the second complex is preceded by the first complex, as seen from the development in the NMR titration.

At a ratio of **PT/3c** = 1:1.5, the aromatic region evolved into sharp assignable signals, while the signals in the negative region coalesced into a broad singlet at $\delta = -4.2$ ppm (Figure 4). Subsequent addition of DABCO (**3c**) gradually shifted the signal further downfield until it was no longer observable at **PT/3c** = 1:2.5. A ^{1}H COSY spectrum of **PT·3c** (1:2) revealed cross-peak signals between the broad signal now at $\delta = -1.6$ ppm with a singlet at 1.8 ppm. This behavior is consistent with a porphyrin–DABCO 2:1 sandwich complex gradually breaking down into a 1:1 complex upon addition of DABCO.[10h]

The titration provided additional insight, as judged by the change of the signals between $\delta = 5$ and 9 ppm (Figure 5). For example, sequential addition of **3c** to complex **PT** gave rise to an upfield shift of the porphyrin H_β signals from $\delta = 8.78$ to 8.35 ppm until 1.5 equivalents had been added. Subsequent addition of **3c** led to a small downfield shift to $\delta = 8.53$ ppm. The signal corresponding to the 3′,5′-MesH protons at $\delta = 6.12$ and 6.16 ppm gradually disappeared as the titration proceeded, thus giving rise to four singlets at $\delta = 6.0$, 6.09, 6.21, and 6.23 ppm upon addition of 1.5 equivalents of **3c**. After subsequent addition of **3c** the signals gradually coalesced back to two signals. Also, a clear change was observed in the signal at $\delta = 9.02$ ppm corresponding to the 4-*H* of the phenanthroline and the aa′ and bb′ signals on **PT**. Upon addition of 1.5 equivalents of **3c**, a new set of signals of equal integrated area corresponding to 4-*H* and aa′ and bb′ was noticed. The signals, upon subsequent addition of **3c**, coalesced into a single set. The above-noted changes point to the transformation of **PT** into **PT·3c** (2:3) upon addition of up to 1.5 equivalents of **3c**, while addition of larger amounts of **3c** led to complex **PT·3c** with a 1:2 composition.

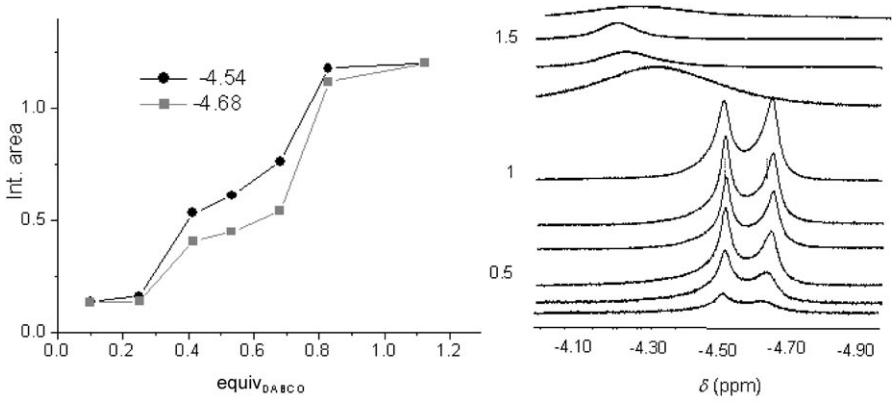

Figure 4. Evolution of the upfield-shifted DABCO signals in the NMR spectra (left) and graphically (right).

UV/Vis investigations: For monitoring the binding of **3a–c** to **PT**, the change in the Soret band of the zinc porphyrin unit of **PT** proved to be of great help.

*Formation of **PT·3a***: During the sequential addition of **3a** to **PT**, the Soret absorption band exhibited a bathochromic shift from 420 to 430 nm due to the axial binding of the pyridyl residues of **3a** to the two zinc porphyrin units of **PT**. The data obtained from the UV/Vis titration were subjected to global

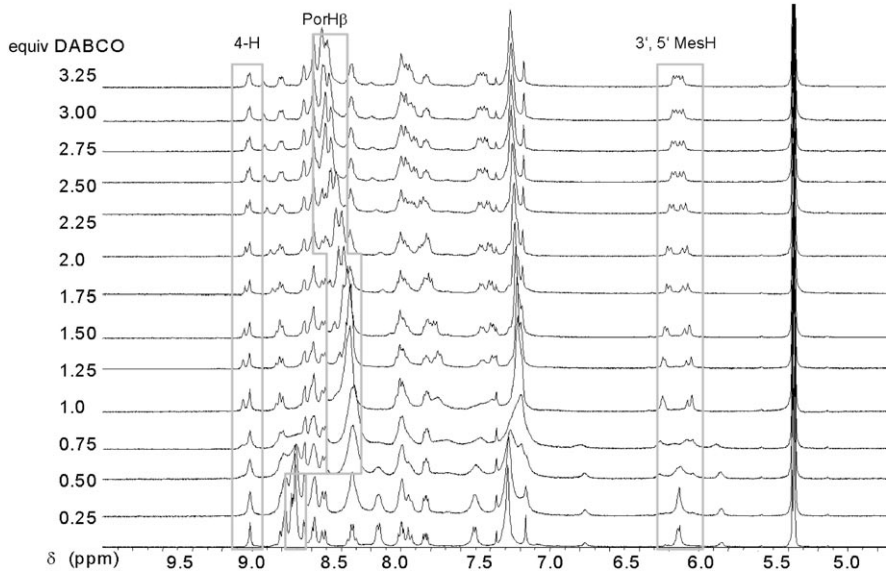

Figure 5. Evolution of the ^{1}H NMR spectra of **PT** upon addition of DABCO (**3c**).

curve fitting by SPECFIT,[17] which provided an association constant for **PT·3a**, that is, logβ of 6.7 ($\pm$0.6) and $K = 5 \times 10^6\,M^{-1}$ (see Table 2). The analysis by both SPECFIT and the Jobs plot supported a 1:1 ratio for **PT·3a** in the final assembly.

*Formation of **PT·3b***: The sequential addition of **3b** to **PT** monitored by UV/Vis spectroscopy displayed a titration profile markedly different from that of the 1:1 adduct **PT·3a**. Noticeably, during the addition of a first equivalent of **3b** the Soret band experienced a bathochromic shift from 420 to 425 nm, while further addition of two equivalents of **3b** shifted it to 430 nm (Figure 6). Jobs plot analysis revealed a 1:1 stoichiometry. Using SPECFIT the best fit was obtained for a 2:2 model with logβ values of 16.4 ($\pm$0.6) for **$(PT)_2$·$(3b)_2$** and 6.4 ($\pm$1.1) for **PT·$(3b)_2$** (see Table 2).[18] The experimental data fitted well to the simulated model of a 2:2 system as shown in Figure 6. The distinctly different NMR profile of **PT·3b** against that of **PT·3a** also supports the proposed model.

Table 2. Macroscopic binding constants obtained from a three-state binding model for **PT** and **3a,b**.

	logβ	K
PT·3a	6.7 ($\pm$0.6)	$5 \times 10^6\,M^{-1}$
PT·$(3b)_2$	6.4 ($\pm$1.1)	$2.5 \times 10^6\,M^{-2}$
PT_2·$(3b)_2$	16.4 ($\pm$0.6)	$2.5 \times 10^{16}\,M^{-3}$

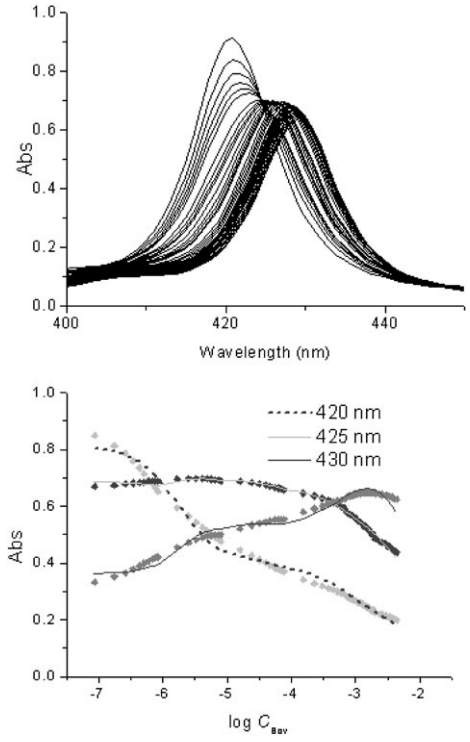

Figure 6. Top: UV/Vis titration profile of **3b** against **PT** at micromolar concentrations. Bottom: Fitting of UV/Vis titration data to a three-state binding model.

*Formation of **PT·3c***: Addition of one equivalent of DABCO (**3c**) to **PT** revealed a characteristic red shift of the Soret band from 420 to 425 nm that was paralleled by analogous red shifts in the Q-band region. Based on earlier studies by Hunter and others,[19] this finding provided tentative evidence for the binding of **3c** within a porphyrin sandwich. To gain further insight, spectrometric titrations were carried out at micromolar concentrations and monitored at the Soret band. The peak at 420 nm corresponding to the unbound zinc porphyrin decreased in intensity, with a new band appearing at 425 nm that is characteristic of a porphyrin·DABCO sandwich complex (Figure 7).[9,10] As the concentration of DABCO increased, the peak at 425 nm decreased with a new maximum emerging at 430 nm which is typical of a simple 1:1 porphyrin·DABCO complex.

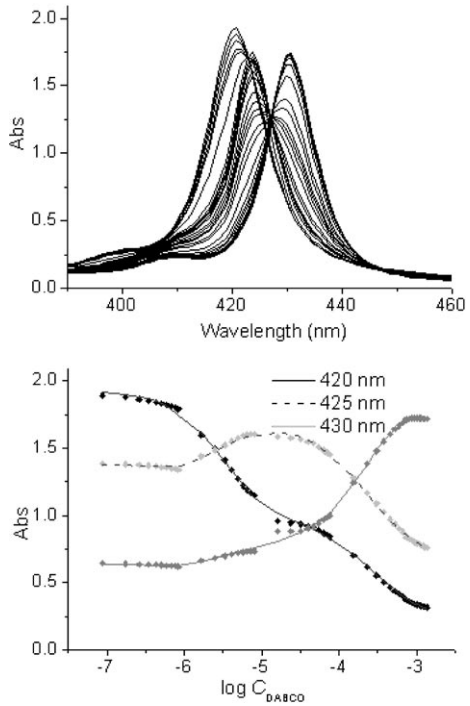

Figure 7. Top: UV/Vis titration of DABCO against micromolar concentrations of **PT**. Bottom: Fitting of UV/Vis titration data to a four-state binding model.

When the titration results were analyzed by SPECFIT,[17] the data fitted best to a 2:3 model providing logβ values of 9.7$\pm$0.2 for **PT·$(3c)_2$**, 15.6$\pm$0.8 for **$(PT)_2$·$(3c)_2$**, and 21.3$\pm$0.4 for **$(PT)_2$·$(3c)_3$** (see Table 3).[20] The 2:3 model is equally

Table 3. Macroscopic binding constants obtained from a four-state binding model for **4**, **PT**, and **3c**.

	logβ	K
4·3c	5.1 ($\pm$0.03)	$1.2 \times 10^5\,M^{-1}$
PT·$(3c)_2$	9.7 ($\pm$0.2)	$5 \times 10^9\,M^{-2}$
$(PT)_2$·$(3c)_2$	15.6 ($\pm$0.8)	$4 \times 10^{15}\,M^{-3}$
$(PT)_2$·$(3c)_3$	21.3 ($\pm$0.4)	$2 \times 10^{21}\,M^{-4}$

supported by the Jobs plot, which gives independently a 1:1.5 mole ratio of **PT** to DABCO, and from the evolution of the signals in the NMR titrations.

In contrast, titration of the simple monoporphyrin complex **4** with **3c** at micromolar concentrations provided a monomeric 1:1 model for the binding of DABCO to porphyrin. The $\log\beta$ value of 5.12 ± 0.03 (K_m) matches well with values known in the literature (see Table 3).[21]

Diffusion NMR studies: To verify beyond doubt the dynamic formation of the three multicomponent assemblies in solution, the aggregates **PT·3a–c** were additionally subjected to diffusion NMR studies. The method to analyze the size/weight of **PT·3a–c** in solution followed that adopted by Reinhoudt, Cohen et al.,[22] which utilized the fact that the ratio of the diffusion coefficients for two different molecular species (D_i/D_j) is inversely proportional to the square root or to the cubic root of the ratio of their molecular weights M_r [Eq. (2)] for rodlike and spherical molecules, respectively.[23] Equation (2) allows determination of the molecular weights of the assemblies under investigation, once a calibration curve that correlates molecular weights and experimentally determined diffusion coefficients of known compounds containing similar structural units has been obtained.

$$\sqrt[3]{\frac{[M_{rj}]}{[M_{ri}]}} \leq \sqrt{\frac{[D_i]}{[D_i]}} \leq \sqrt{\frac{[M_{rj}]}{[M_{ri}]}} \qquad (2)$$

Table 4 shows the experimental diffusion coefficients measured for structures **4**, **PT**, and **PT·3a** as well as for **PT·3b** and **PT·3c** in various proportions. By inserting the diffusion coefficient values for **PT** into Equation (2), two theoretical calibration curves for molecular weights between 0 and 10000 a.m.u. were obtained with **PT** as anchor point (Figure 8). The calibration was nicely confirmed by having

Table 4. Experimental diffusion coefficients measured in CD_2Cl_2 at 298 K and their respective molecular weights.

Composition of the mixture (mol equivalent)	Experimental diffusion coefficient [10^{-10} m^2 s^{-1}]	Possible aggregates and their molecular weight [g mol^{-1}]
4 (1 equiv)	12.2	1725/**4**
PT (1 equiv)	9.2	3940/**PT**
PT (1 equiv) and **3a** (1 equiv)	9.4	4276/**PT·3a**
PT (1 equiv) and **3b** (1 equiv)	6.2	4096/**PT·3b**; 8192/**(PT)$_2$·(3b)$_2$**
PT (1 equiv) and **3b** (2 equiv)	12.2	4252/**PT·(3b)$_2$**
PT (1 equiv) and **3c** (1 equiv)	5.5	4052/**PT·3c**; 8104/**(PT)$_2$·(3c)$_2$**
PT (1 equiv) and **3c** (1.5 equiv)	7.3	8216/**(PT)$_2$·(3c)$_3$**
PT (1 equiv) and **3c** (2 equiv)	8.9	4164/**PT·(3c)$_2$**

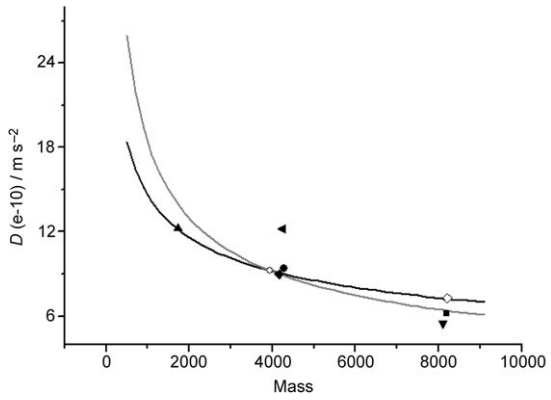

Figure 8. Graphical analysis of diffusion coefficients D versus molecular weight M. The solid lines represent the theoretical correlation of diffusion coefficients and molecular weights as a function of the two models [sphere (black) or rod (gray)] according to Equation (a), while the dots represent various compositions of the self-assemblies. **4** (▲); **PT** (○); **(PT)$_2$·(3c)$_2$** (▼); **(PT)$_2$·(3c)$_3$** (◇); **PT·(3c)$_2$** (◆) formed at excess of **3c**; **(PT)$_2$·(3b)$_2$** (■); **PT·(3b)$_2$** (◀) formed at excess of **3b**; **PT·3a** (●).

the diffusion coefficient of **4** (▲) falling right on the black curve. Importantly, all experimental diffusion coefficients for the other aggregates fitted the calibration curves only for those stoichiometries suggested by the Jobs plot and UV/Vis titration global simulation results. Accordingly, mixing **PT** and **3a** in a ratio of 1 equiv:1 equiv afforded an aggregate **PT·3a** (1:1) with a molecular weight of 4276 a.m.u (●). In contrast, mixing **PT** and **3b** in a ratio of 1 equiv:1 equiv furnished an aggregate with a molecular weight of 8192 a.m.u (■) that is in agreement with **(PT)$_2$·(3b)$_2$**, while a mixture of 1 equiv:2 equiv led to **PT·(3b)$_2$** with a reduced molecular weight (◀). Similarly, the aggregates formed by mixing **PT** and **3c** in ratios of 1 equiv:1 equiv or 1 equiv: 1.5 equiv fit the calibration curve only with molecular weights around 8100 a.m.u, that is, **(PT)$_2$·(3c)$_2$** and **(PT)$_2$·(3c)$_3$**, respectively. Since the difference between the molecular weights of the 2:3 and 2:2 compositions amounts to only 112 a.m.u, the difference is not well resolved in the DOSY spectra. When the ratio of **PT** and **3c** was increased to 1 equiv:2 equiv, only the small aggregate **PT·(3c)$_2$** with a molecular weight of 4164 a.m.u emerged.

Based on the proof from UV spectroscopy, NMR titrations, and DOSY, the composition of a double sandwich assembly was ascertained in the case of **PT·3b** and **PT·3c** as against the 1:1 adduct in the case of **PT·3a**. Moreover, as is noticeable from the single set of signals seen in the 2D DOSY plots (Figures S19–S25 in Supporting Information), each **PT·3** assembly showed up as a clean species without any side products of lower molecular weight.

Inferences

***PT**: a dynamic supramolecular tweezer*: As against a number of known examples of covalent porphyrin tweezers,[24] **PT** represents the first example of a supramolecular porphyrin tweezer. The use of Cu^I-directed heteroleptic phenanthro-

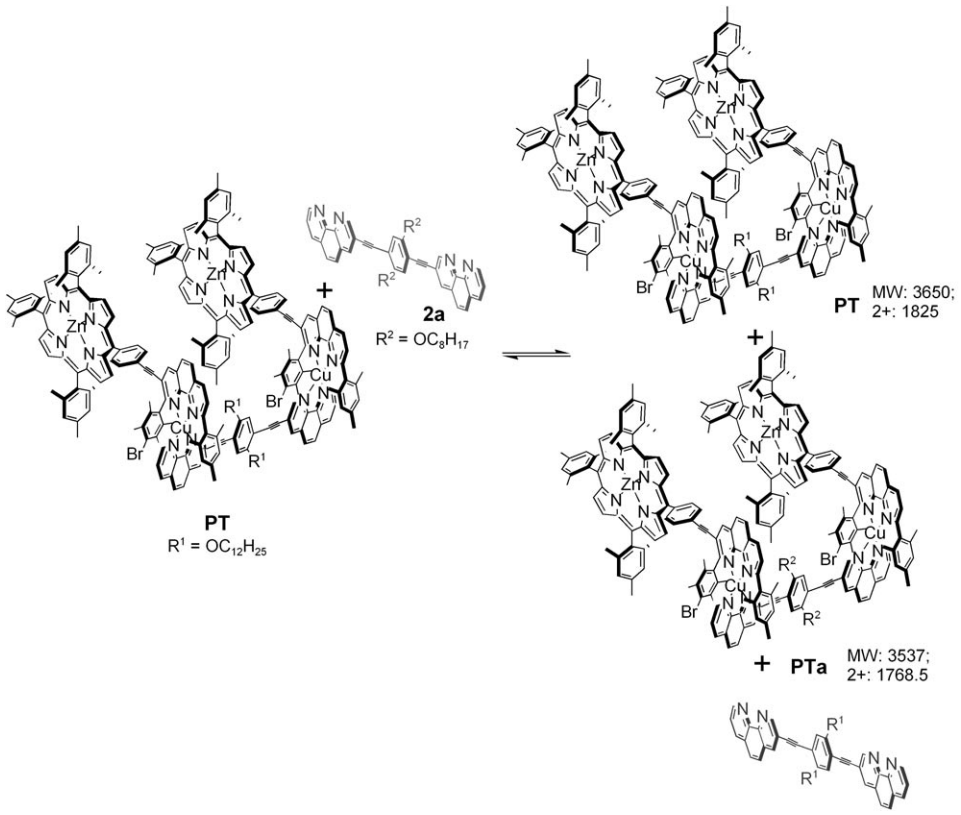

Figure 9. Investigations on the dynamic nature of **PT**.

line complexation enables exclusive formation of **PT** as a dynamic assembly, as tested by ligand exchange experiments (Figure 9). Thus, when a solution of **PT** was titrated against ligand **2a**, a bisphenanthroline analogue of **2** with a shorter alkoxy side chain, a facile exchange of the bisphenanthroline ligands was observed after five minutes which provided a mixture of two tweezers **PT** and **PTa**. The ligand exchange was monitored by ESI-MS through the gradual increase in the relative abundance of the dication of **PTa** at m/z 1768.5 (Figure S3 in Supporting Information).

The macroscopic binding constant for the formation of **PT** was calculated from UV/Vis titrations by addition of aliquots of Cu^{I} to a solution of **1** and **2** (2:1 ratio). The formation of the complex was accompanied by a distinct decrease in the intensity of the Soret band at 420 nm along with the appearance of a low and broad absorption at 420–525 nm, which is a characteristic metal-to-ligand charge transfer (MLCT) band for a Cu^{I} complex (Figure S14 in Supporting Information). The association constant was $\log\beta = 20.1 \pm 0.6$ ($K = 1.1 \times 10^{20}\,\text{M}^{-4}$).

*Formation of **PT·3a** (1:1)*: The combined UV/Vis, NMR, and diffusion NMR spectroscopy results bear witness to a remarkable structural reorganization of **PT** as a function of the added bis-nitrogen spacers **3a–c**. In the presence of **3a**, the dynamic bis-porphyrin tweezer **PT** operates as a supramolecular bidentate host ($d_{ZnZn} \cong 19$ Å) for the bidentate guest molecule **3a** ($d_{NN} = 16$ Å) due to a nearly perfect geometric complementarity of the two constituents, which gives rise to the formation of the 1:1 aggregate **PT·3a** (Figure 10). As a result of a lack of configurational control in the formation of **PT** and **PT·3a**, however, we expect the formation of two diastereomeric assemblies, namely, *meso*- and *rac*-**PT·3a**. Interestingly, the NMR analysis of the diagnostic 3′,5′-MesH protons in **PT·3a**, although impeded by the nearly isochronous signals of the two diastereomeric aggregates, shows a clear preference for one diastereomer (ca. 4:1 excess), in contrast to the situation in **PT** where a diastereomeric ratio of 1:1 is registered. The presence of two diastereomeric aggregates is also registered by the appearance of two closely placed signals for the 4-H and Hb,Hb′ protons of **1**. Association constants derived for **PT**+**3a**→**PT·3a** revealed a $\log\beta$ value of 6.7 (± 0.6) and hence an association constant $K = 5 \times 10^{6}\,\text{M}^{-1}$. This value is typical for ditopic interactions of a bis-porphyrin system with a bis-nitrogen ligand.[25] The magnitude of the association constant in this case is largely independent of any cooperativity effects, thus amounting to about twice that of the association of the parent pyridine to ZnTPP ($2 \times \log\beta_{py} = 2 \times 3.8 = 7.6$; TPP = tetraphenylporphyrin).[26]

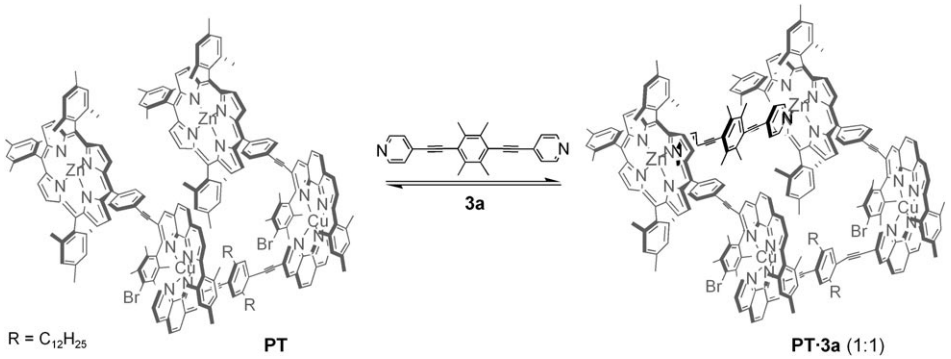

Figure 10. Formation of **PT·3a** (1:1) from the reaction of **3a** with **PT**.

*Formation of **PT·3b** (2:2)*: Although the distance between the two zinc porphyrins in **PT** ($d_{ZnZn} \cong 19$ Å) can be modulated to some extent by a distortion about the two Cu^{I} bis-phenanthroline complexation sites, it is expected to become enthalpically less favorable to coordinate a much smaller bis-nitrogen spacer, such as **3b** ($d_{NN} = 7$ Å), in a 1:1 adduct. As such, it was not astonishing to find exclusively the 2:2 dimeric assembly **$(PT)_2$·$(3b)_2$** from the reaction of one equivalent of **PT** with one equivalent of **3b** (Figure 11). This assignment is unequivocally supported by combined evidence from the UV/Vis and NMR titrations and the DOSY experiments.

While the above results confirm the 2:2 composition of **$(PT)_2$·$(3b)_2$**, they do not provide a complete picture of its structure in solution. This is due to the fact that the dynamic nature of the assembly would allow for multiple conformations with the same composition (see Figure 12).

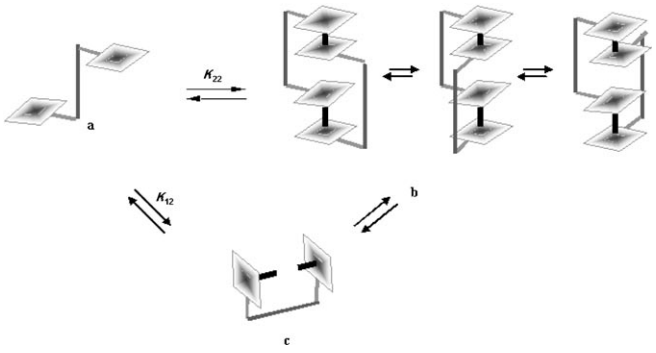

Figure 12. Coordination and conformational equilibria present in a mixture of **PT** and **3b**.

*Formation of **PT·3c** (2:3)*: A further decrease of the size of the bis-nitrogen spacer down to 3 Å by using **3c** (DABCO) produced the unexpected 2:3 aggregate **$(PT)_2$·$(3c)_3$**, as indicated by the Jobs plot and NMR analysis. At first an analogous 2:2 assembly similar to **$(PT)_2$·$(3b)_2$** had been expected, but the internal cavity produced by a 2:2 complex offers an optimal-sized bis(zinc porphyrin) complexation site for the inclusion of a third molecule of **3c**. However, the attachment of a sixth ligand at the zinc atom is known to labilize and destabilize the already bound axial ligand, and consequently association complexes of the type DABCO–(zinc porphyrin)–DABCO have only been observed in the solid state[27] and never in solution. Thus, binding of the third molecule of **3c** is expected to weaken and break down the 2:2 aggregate **$(PT)_2$·$(3c)_2$**. The double-sandwich aggregate, however, does not show any indications of breaking down at the mole ratio of 1:1.5 (**PT:3c**), as in the ^{1}H NMR spectrum the porphyrin H_β protons maintain the upfield shift position. Furthermore, the two signals corresponding to the 3′,5′-MesH protons continue to appear as four separate signals due to the nonequivalence of these protons. Hence, by virtue of the appropriately spaced porphyrins, the aggregate dynamically creates a binding site which anomalously accepts a third DABCO guest, contrary to known linear bis-porphyrins which only assemble in a 2:2 sandwich composition.[10a,h] Thus, it can be concluded that there is a fast equilibration of the three DABCO molecules, which keeps the "double Pac-Man" porphyrin framework intact (Figure 13). A distinct assignable set of NMR signals for the aromatic region at 2:3 stoichiometry (Figure S11 in Supporting Information) provides evidence for the same.

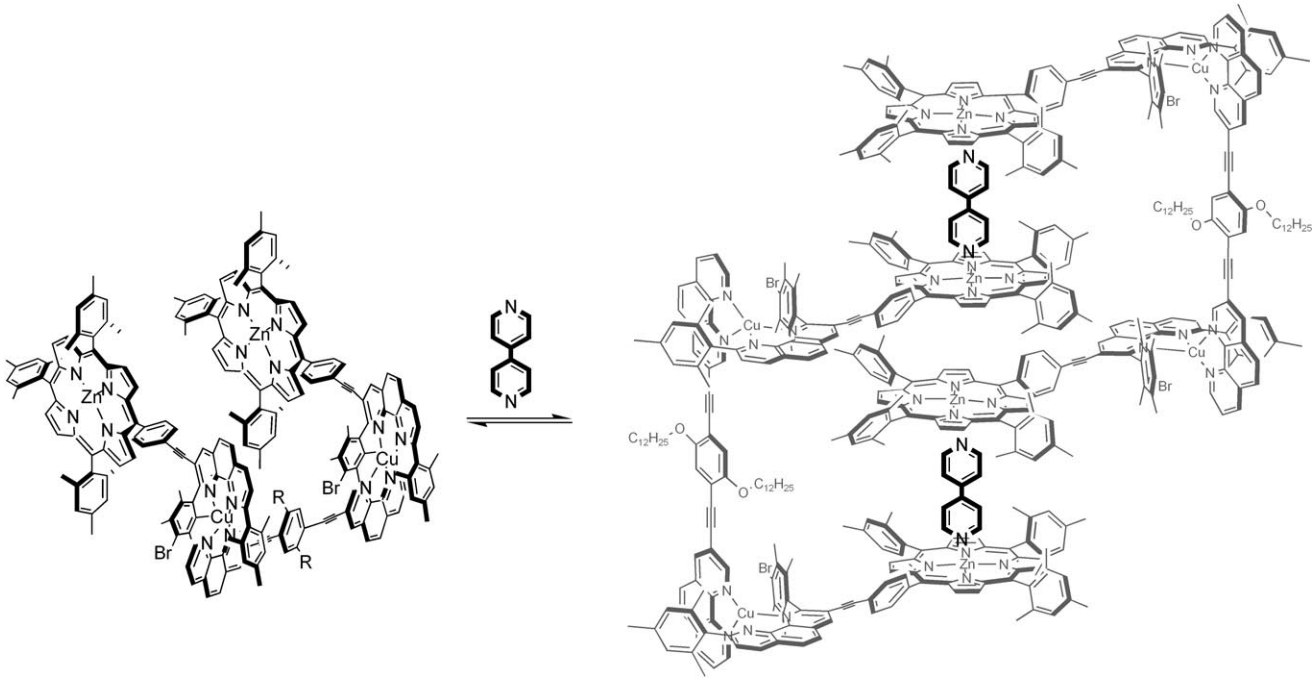

Figure 11. Formation of the 2:2 dimeric assembly **$(PT)_2$·$(3b)_2$** from the reaction of **3b** with **PT**.

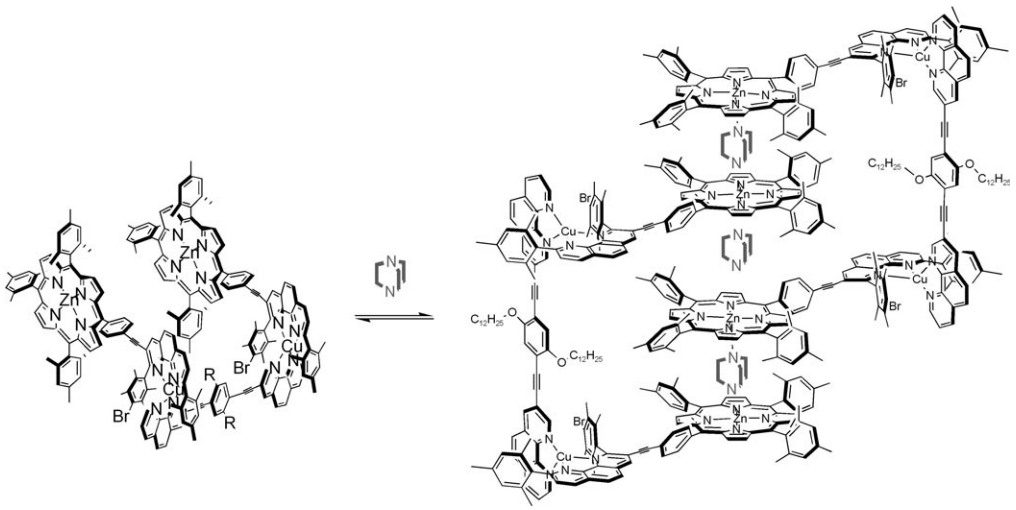

Figure 13. Proposed chemical structure of the 2:3 aggregate $\mathbf{(PT)_2{\cdot}(3c)_3}$.

On the basis of the experimental binding constants, a simple model could be proposed for the dynamics observed in the system **PT**+**3c** (Figure 14). The value of K_m was calculated from K_{12} to be $\log\beta = 4.6$, close to the value obtained in the titration of **4** to DABCO. From the value of K_{22} it is possible to calculate E_m (effective molarity) which is found to be 0.002 M.

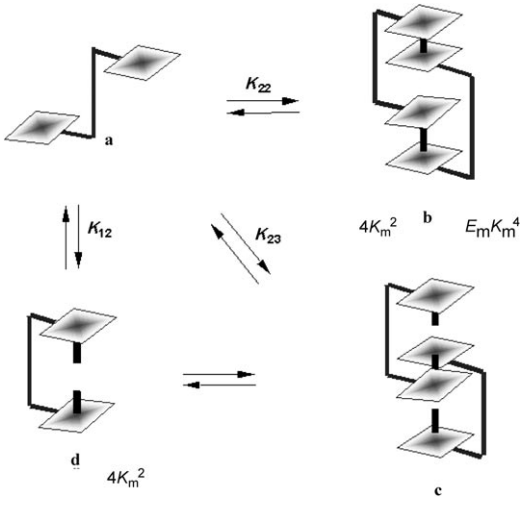

Figure 14. Equilibria present in a mixture of **PT** and DABCO.

The veracity of the model in Figure 14 was further interrogated by fitting the NMR titration data to the simulated concentration profiles for a 2:3 model obtained from the UV titration (Figure 15). The NMR data fit agreeably to the concentration profile. The concentration profile also reveals that the 2:2 complex shows 100% formation, while the 2:3 complex is never completely formed and breaks down on addition of excess of **3c** (DABCO). Since the mass difference between the 2:3 and 2:2 complexes is only 112 (molecular weight of one DABCO molecule), the DOSY experiment does not distinguish the two species and thus provides a single value for the diffusion coefficient.

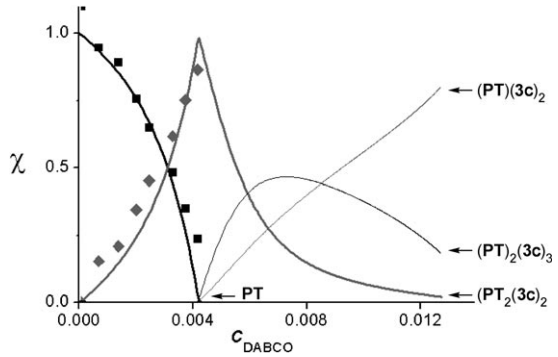

Figure 15. Fitting of NMR titration data to concentration profiles of a 2:3 binding model obtained from the UV/Vis titration. The plot depicts the changes in the mole fraction (χ) of the four different species against the concentration of DABCO: free **PT**; 2:2 aggregate $\mathbf{(PT)_2{\cdot}(3c)_2}$; 2:3 aggregate $\mathbf{(PT)_2{\cdot}(3c)_3}$; 1:2 aggregate $\mathbf{PT{\cdot}(3c)_2}$. The symbols represent the experimental values as observed from NMR titration.

As in the case of **PT·3b**, the experimental studies allow the composition to be determined unequivocally, but due to the dynamic nature of the complex configurational issues have to remain unaddressed.

One-pot approach to the four-component assemblies: The foregoing discussion demonstrates the successful formation of four-component assemblies in a stepwise process, that is, by the initial formation of a three-component assembly **PT** that develops into tertiary assemblies by the coordination of bases **3a–c**. Importantly, all assemblies could equally be prepared in one-pot reactions, where all components were put together as solids and then brought into solution by dissolving them in dichloromethane (Figure 16). The resulting solution was then tested by NMR and UV/Vis spectroscopy. The

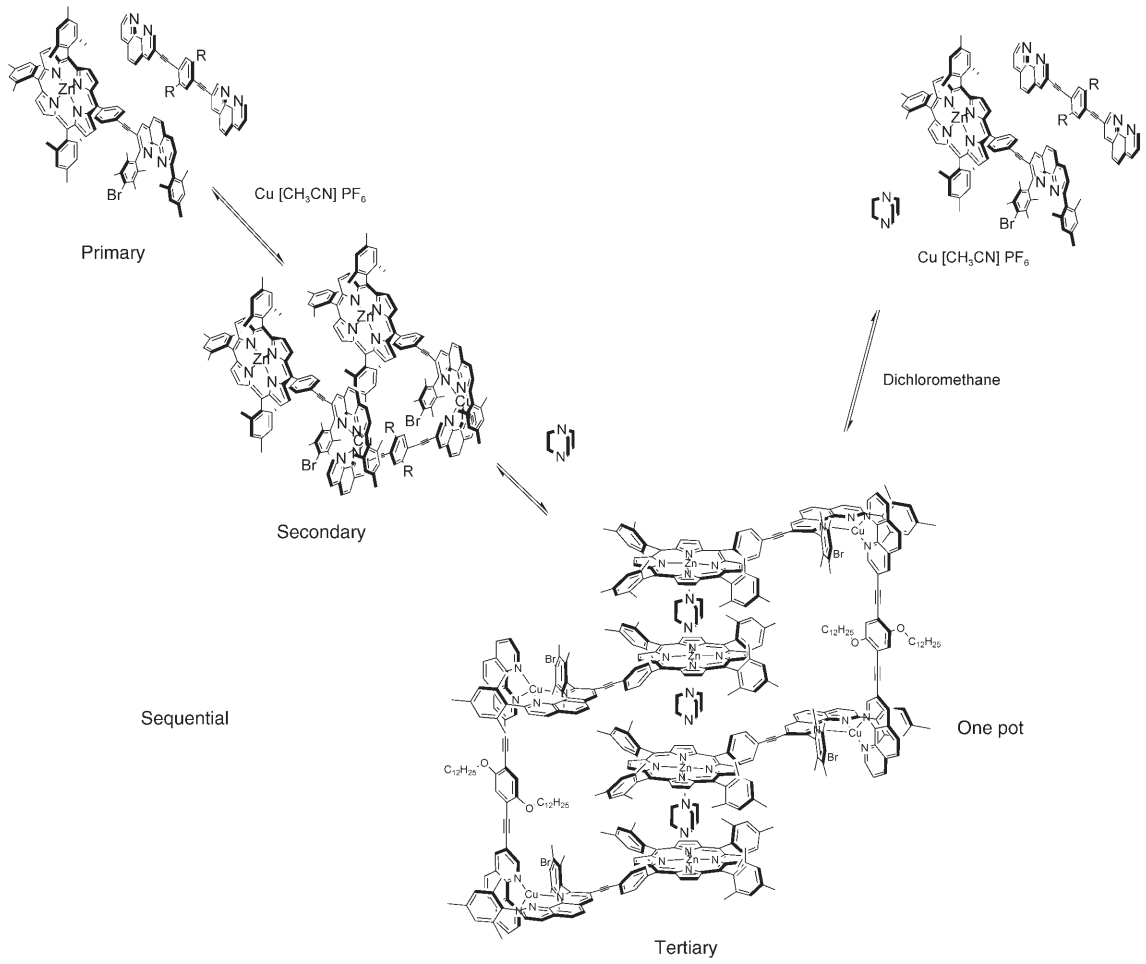

Figure 16. Hierarchy of self-assembly processes leading to a tertiary structure.

^{1}H NMR spectra were exactly the same as those obtained in a stepwise approach. The final proof of the formation of the same structural composition was obtained by performing a DOSY experiment, which yielded the same diffusion coefficients. This result led us to conclude that the same supramolecular composition could be achieved by either a one-pot or a sequential approach owing to the noninterfering nature of the two binding algorithms.

Conclusion

In summary, we provide a unique example of the translation of a set of simple covalent components into a tertiary assembly obtained through a binary binding algorithm, with two noninterfering binding interactions driving the system thermodynamically into a unique supramolecular assembly. We demonstrate that careful tuning of components at a lower level of a multicomponent assembly (the length of one of the components in the present case) could translate into substantial changes in the structure of the assembly.

In moving toward highly functional multimolecular aggregates, there is a need to introduce further complexity in an organized manner to the present generation of supramolecules. A logical step in this direction would be to utilize supramolecules themselves as building blocks to build tunable and meaningful tertiary superstructures. This would call for the use of more than one kind of noncovalent interactions (which are noninterfering and orthogonal) and multiple molecular components (typically $\geq$four) in the self-assembly. Our future investigations aim at exploring this aspect further.

Experimental Section

Porphyrin **1** and bisphenanthroline **2** were synthesized by known procedures from earlier reports.[7d,13] **3a** was synthesized based on an analogous report.[14] DABCO and 4,4′-bipyridine were obtained from ACROS Chemicals. $[Cu(MeCN)_4]PF_6$ was prepared according to known procedures.[28] ^{1}H NMR spectra were recorded on a Bruker AC 400 (400 MHz) or Bruker AC 200 (200 MHz) spectrometer and ^{13}C NMR spectra were obtained on a Bruker AC 400 (100 MHz) or Bruker AC 200 (60 MHz) instrument. ^{1}H NMR spectroscopy was carried at room temperature in CD_2Cl_2. ESI-MS was performed on an LCQ Deca ThermoQuest instrument. Typically, 25 scans were accumulated for one spectrum. All complexes were characterized by ^{1}H NMR, ^{13}C NMR, and elemental analysis.

Zinc(II) *meso*-5-{4-[3-(2-(4-bromo-2,3,5,6-tetramethyl)-9-(2,4,6-trimethylphenyl))-1,10-phenanthrolin-3-ylethynylethynyl]phenyl}porphyrin (1): In a three-necked round-bottomed flask fitted with a reflux condenser, *meso*-5-(4-iodophenyl)-10,15,20-trimesityl zinc porphyrin (138 mg, 148 μmol) was taken up in dry benzene/triethylamine (20 mL, 15:5). Then 3-[2-(2,4,6-trimethylphenyl)-9-(4-bromo-2,3,5,6-tetramethyl)-1,10-phenanthrolinyl]ethyne (79.0 mg, 148 μmol) was added to this solution. The mixture was degassed for 30 min under a steady flow of nitrogen. $[Pd_2(dba)_3]$ (10.0 mg, 1.48 μmol) and $AsPh_3$ (45.3 mg, 148 μmol) were then added as solids. The reaction was heated at 40 °C for 4 h, after which the reaction mixture was evaporated in a vacuum. The residue obtained was dissolved in dichloromethane and washed with a solution of 2% KCN dried over sodium sulfate. The resulting solid was chromatographed on silica gel with dichloromethane as eluent to give a violet solid containing **1** as a crude product. The solid was then dissolved in toluene (1 mL), the solution was loaded on a size-exclusion gel containing BioRad Bio-Beads SX-1 swollen in toluene, and a chromatography run was carried out under gravity flow. The bright red fractions were isolated to give the product. Yield: 85 mg (43%); ^{1}H NMR (400 MHz, CD_2Cl_2): $\delta = 8.88$ (d, $J = 4.5$ Hz, 2H; pyrrol-H1), 8.81 (d, $J = 4.5$ Hz, 2H; pyrrol-H2), 8.77 (d, $J = 4.5$ Hz, 4H; pyrrol-H3, -H4), 8.68 (s, 1H; 4-H), 8.35 (d, $J = 8.2$ Hz, 1H; 7-H), 8.20 (d, $J = 7.9$ Hz, 2H; Ar-Hb, -Hb′), 7.96 (s, 2H; 5-, 6-H), 7.64 (d, $J = 8.2$ Hz, 1H; 8-H), 7.53 (d, $J = 7.9$ Hz, 2H; Ar-Ha, -Ha′), 7.33 (s, 6H; por-mes-H), 7.01 (s, 2H; 3‴-, 5‴-H), 2.68 (s, 9H; por-mes-Me), 2.59 (s, 6H; 8″-, 9″-H), 2.39 (s, 3H; 8‴-H), 2.23 (s, 6H; 7‴-, 9‴-H), 2.20 (s, 6H; 7″-, 10″-H), 1.92 (s, 9H; por-mes-Me), 1.90 ppm (s, 9H; por-mes-Me); ^{13}C NMR (100 MHz, $CDCl_3$): $\delta = 163.0$, 161.1, 150.3, 150.1, 149.9, 146.3, 145.2, 144.3, 143.8, 140.7, 139.7, 138.9, 138.4, 138.0, 137.7, 136.5, 135.1, 134.9, 134.2, 133.8, 132.1, 131.5, 131.1, 130.9, 130.0, 129.7, 129.3, 128.9 ,128.8, 128.7, 128.0, 127.6, 127.4, 127.1, 126.1, 125.7, 122.0, 120.7, 119.2, 119.1, 96.3, 88.1, 22.2, 21.8, 21.5, 21.4, 21.0, 19.2, 18.7, 14.6 ppm; ESI-MS: *m*/*z* (%): 1335.9 (100) $[M+H]^+$; elemental analysis (%) calcd for $C_{86}H_{73}BrN_6Zn$: C 77.32, H 5.51, N 6.29; found: C 77.74, H 5.68, N 6.28.

1,4-Bis(4′-pyridylethynyl)durene (3a): In a two-necked round-bottomed flask fitted with a reflux condenser, 1,4-diiododurene (138 mg, 357 μmol), 4-ethynylpyridine hydrochloride (120 mg, 859 μmol), $[Pd(PPh_3)_2Cl_2]$ (7.50 mg, 10.6 μmol), and copper iodide (10 mg, 52 μmol) were mixed under a nitrogen atmosphere. Benzene (10 mL) and diethylamine (5 mL) were added to the flask. The reaction mixture was refluxed for 12 h, after which the solvents were removed and the residue was dissolved in toluene and eluted over a pad of silica. The resulting light yellow solution was evaporated to give a yellow solid **3a**. Yield: 180 mg (68%); ^{1}H NMR (400 MHz, CD_2Cl_2): $\delta = 8.63$ (dd, $^3J = 4.5$ Hz, $^4J = 1.6$ Hz, 4H), 7.41 (dd, $^3J = 4.5$ Hz, $^4J = 1.6$ Hz, 4H), 2.51 ppm (12H; CH_3); ^{13}C NMR (100 MHz, $CDCl_3$): $\delta = 149.7$, 136.3, 131.7, 125.3, 123.1, 95.5, 92.9, 18.3 ppm; ESI-MS: *m*/*z* (%): 337.4 (100) $[M+H]^+$; elemental analysis (%) calcd for $C_{24}H_{20}N_2$: C 85.68, H 5.99, N 8.33; found: C 85.38, H 5.87, N, 8.70.

Complex 4: Anhydrous 1,10-phenanthroline (1 equiv) was added to equimolar amounts of **1** and $[Cu(CH_3CN)_4]PF_6$ in dichloromethane. The resulting solution showed an instantaneous change in color to deep red. The complex was isolated without any further purification and was found to be **4**, obtained in quantitative yield. ^{1}H NMR (400 MHz, CD_2Cl_2): $\delta =$ 8.95 (s, 1H; 4-H), 8.72 (d, $J = 7.8$ Hz, 1H; 7-H), 8.72 (d, $J = 4.6$ Hz, 2H; pyrrol-H1), 8.68 (d, $J = 4.8$ Hz, 2H; pyrrol-H3), 8.67 (d, $J = 4.8$ Hz, 2H; pyrrol-H4), 8.66 (d, $J = 4.6$ Hz, 2H; pyrrol-H2), 8.52 (dd, $^3J = 4.6$ Hz, $^4J =$ 1.3 Hz, 2H; 2′-, 9′ -H), 8.44 (dd, $^3J = 8.1$ Hz, $^4J = 1.5$ Hz, 2H; 4′-, 7′-H), 8.27 (d, $J = 9.1$ Hz, 1H; 5-H), 8.24 (d, $J = 9.1$ Hz, 1H; 6-H), 8.08 (d, $J =$ 8.2 Hz, 2H; Ar-Ha, -Ha′), 7.92 (s, 2H; 5′-, 6′-H), 7.91 (d, $J = 7.8$ Hz, 1H; 8-H), 8.27 (dd, $^3J = 8.0$ Hz, $^3J = 4.8$ Hz, 2H; 3′-, 8′-H), 7.44 (d, $J = 8.2$ Hz, 2H; Ar-Hb, -Hb′), 7.26 (s, 6H; por-mes), 6.02 (s, 2H; 3‴-, 5‴-H), 2.59 (s, 12H; 7″-, 10″-, 7‴-, 9‴-H), 1.81 (s, 18H; por-mes-Me), 1.78 (s, 9H; por-mes-Me), 1.64 (s, 6H; 8″-, 9″-H), 1.54 ppm (s, 3H; 8‴-H); ^{13}C NMR (100 MHz, CD_2Cl_2): $\delta = 160.5$, 159.0, 149.4, 149.2, 149.2, 148.9, 147.2, 144.4, 143.4, 142.4, 141.8, 139.0, 138.9, 138.5, 137.3, 136.9, 135.9, 134.2, 132.8, 131.8, 131.0, 130.4, 130.1, 129.1, 128.3, 127.8, 127.3, 127.1, 126.6, 126.4, 125.8, 124.2, 122.3, 120.0, 118.1, 117.9, 97.0, 85.3, 21.1, 20.7, 19.6, 19.5 (2), 19.4 (2), 17.7 ppm; ESI-MS: *m*/*z* (%): 1579.6 (100) $[M]^+$; elemental analysis (%) calcd for $C_{98}H_{81}BrCuF_6N_8PZn$: C 68.25, H 4.73, N 6.50; found: C 68.77, H 4.68, N 6.56.

Complex PT: Bisphenanthroline **2** (0.5 equiv) was added to a solution of **1** and $[Cu(CH_3CN)_4]PF_6$ (1:1 in dichloromethane). The deep red solution obtained was evaporated and complex **PT** was isolated in quantitative yield. ^{1}H NMR (400 MHz, CD_2Cl_2): $\delta = 8.96$ (s, 2H; 4-H), 8.75 (d, $J =$ 8.3 Hz, 2H; 7-H), 8.72 (d, $J = 4.5$ Hz, 2H; pyrrol-H1), 8.68 (d, $J = 4.8$ Hz, 2H; pyrrol-H3), 8.67 (d, $J = 4.8$ Hz, 2H; pyrrol-H4), 8.66 (d, $^3J = 4.6$ Hz, 2H; pyrrol-H2), 8.61 (d, $^4J = 1.5$ Hz, 2H; 4′-H), 8.54 (d, $^4J = 1.5$ Hz, 4H; 2′-H), 8.53 (d, $^4J = 1.5$ Hz, 2H; 9′-H), 8.47 (d, $J = 8.3$ Hz, 4H; 7′-H), 8.29 (d, $J = 9.1$ Hz, 1H; 5′-H), 8.25 (d, $J = 9.1$ Hz, 1H; 6′-H), 8.08 (d, $J =$ 7.7 Hz, 4H; Ar-Ha, -Ha′), 7.95 (d, $J = 8.1$, 1H; 8-H), 7.94 (d, $J = 9.1$ Hz, 1H; 5-H), 7.89 (d, $J = 9.1$ Hz, 1H; 6′-H), 7.78 (dd, $^3J = 8.1$ Hz, $^3J = 4.8$ Hz, 2H; 8′-H), 7.45 (d, $J = 7.7$ Hz, 4H; Ar-Hb, -Hb′), 7.26 (s, 6H; por-mes-Ha), 7.24 (s, 6H; por-mes-Hb), 7.12 (s, 2H; phenyl-H), 6.11 (s, 2H; 3‴-, 5‴-H1), 6.07 (s, 2H; 3‴-, 5‴-H2), 4.03 (t, $J = 6.2$ Hz, 4H; OCH_2), 2.59 (s, 12H; 7″-, 9″-H), 2.56 (s, 12H; 7‴-, 10‴-H),1.92 (s, 6H; por-CH_3), 1.89 (s, 6H; por-CH_3), 1.85 (s, 6H; por-CH_3), 1.80 (s, 18H; por-CH_3), 1.76 (s, 18H; por-CH_3), 1.62 (s, 6H; 8‴-H), 1.59 (s, 12H; 8″-, 9″-H), 1.17 (m, 40H; OCH_2-$C_{10}H_{20}$-CH_3), 0.82 ppm (t, $J = 6.8$ Hz, 6H; $OC_{11}H_{22}$-CH_3); ^{13}C NMR (100 MHz, CD_2Cl_2): $\delta = 185.4$, 161.3, 159.9, 154.3, 150.3, 150.0, 149.7, 149.5, 148.4, 144.7, 144.1, 142.9, 142.6, 141.6, 140.2, 140.2, 139.9, 139.4, 139.3, 139.2, 139.1, 138.3, 137.9, 137.7, 137.0, 135.1, 135.0, 134.9, 133.8, 132.7, 132.6, 131.8, 131.5, 131.4, 130,9,130.0, 129.7, 129.4,129.2,128.6, 128.4, 127.9, 127.6, 127.2, 126.8, 126.6, 125.2, 123.2, 121.8, 121.0, 119.6, 119.3, 118.9, 117.0, 113.8, 111.3, 110.8, 97.9, 92.4, 90.9, 86.1, 84.9, 69.8, 32.2, 30.0, 29.9, 29.7, 29.6, 26.3, 23.1, 21.8, 21.7, 21.5, 20.5, 20.5, 20.3, 18.7, 18.6, 14.3 ppm; ESI-MS: *m*/*z* (%): 1824.9 (100) $[M]^{2+}$; elemental analysis (%) calcd for $C_{230}H_{212}Br_2Cu_2F_{12}N_{16}O_2P_2Zn_2$: C 70.12, H 5.42, N 5.69; found: C 70.35, H 5.42, N 6.22.

Complexes PT-3a–c: **PT-3a–c** were prepared by adding the respective equivalents of **3a–c** to **PT** in CH_2Cl_2. For NMR purposes, the complex was prepared by adding **3a–c** directly to an NMR tube containing **PT**, and subsequent measurements were made without any further isolation or purification. Extensive characterization is described in the Results section.

Titrations: UV/Vis titrations were performed on a Cary Varian UV instrument with a quartz cuvette of path length 1.0 cm at 25 °C in CH_2Cl_2. Aliquots of millimolar concentrations of bases **3a**, **3b**, and **3c** were added to complex **PT** at micromolar concentrations with microliter syringes. UV/Vis titrations were analyzed by fitting the whole series of spectra at 0.5-nm intervals using the software SPECFIT version 3.0.22 (Spectrum Software Associates, P.O. Box 4494, Chapel Hill, NC 27515-4494, USA), which uses a global analysis system with expanded factor analysis and a Marquardt least-squares minimization to obtain globally optimized parameters.[29]

^{1}H NMR titrations were performed in CD_2Cl_2 in a 5-mm NMR tube at 298 K on a Bruker AC 400 (400 MHz) instrument by sequential addition of the bases into the NMR tube with a microliter syringe.

DOSY: Diffusion experiments were performed on the Bruker Avance 400-MHz NMR spectrometer, with a 5-mm BBI probe head, equipped with a pulsed field gradient unit capable of producing magnetic field gradients in the *z* direction of about 5.35 Gcm^{-1}. All experiments were carried out at 298 K in a 5-mm NMR tube at 2 mM concentration. The bipolar magnetic field pulse gradients (δ) were of 2.5–4.5 ms duration, and the diffusion time (Δ) was 50 ms. The pulse gradients were increased from 0.10 to 5.08 Gcm^{-1} in 32 steps. Signals were averaged over 30–45 scans. In each experiment the peaks were analyzed using an inbuilt intensity fit function "simfit" which utilizes Equation (3)], where γ is the gyromagnetic radius ($rad\,s^{-1}\,G^{-1}$), δ is the length of the diffusion gradients ($G\,cm^{-1}$), Δ is the time of separation between the gradients, G is the pulsed gradient strength, and D is the diffusion coefficient.

$$I = I(0)\ e[D(-\gamma^2 G^2 \delta^2)(\Delta - \delta/3)] \qquad (3)$$

Acknowledgements

We are very much indebted to the DFG and the Fonds der Chemischen Industrie for continued financial support.

[1] J.-M. Lehn in *Nobel Lectures, Chemistry (1981–1990)* (Ed.: B. G. Malmström), World Scientific Publishing Co., Singapore, **1992**.

[2] a) S. Leininger, B. Olenyuk, P. J. Stang, *Chem. Rev.* **2000**, *100*, 853–907; b) J.-M. Lehn, *Supramolecular Chemistry: Concepts and Perspectives*, VCH, Weinheim, **1995**; c) J. W. Steed, J. L. Atwood, *Supramolecular Chemistry*, Wiley, New York, **2001**; d) A. V. Davis, R. M. Yeh, K. N. Raymond, *Proc. Natl. Acad. Sci. USA* **2002**, *99*, 4793–4796; e) D. L. Caulder, K. N. Raymond, *Acc. Chem. Res.* **1999**, *32*, 975–982; f) J. A. R. Navarro, B. Lippert, *Coord. Chem. Rev.* **1999**, *185–186*, 653–667; g) R.-D. Schnebeck, E. Freisinger, B. Lippert, *Angew. Chem.* **1999**, *111*, 235–238; *Angew. Chem. Int. Ed.* **1999**, *38*, 168–171; h) M. Fujita, *Acc. Chem. Res.* **1999**, *32*, 53–61.

[3] a) Y. L. Cho, H. Uh, S.-Y. Chang, H.-Y. Chang, M.-G. Choi, I. Shin, K.-S. Jeong, *J. Am. Chem. Soc.* **2001**, *123*, 1258–1259. (Host–guest supramolecular systems which are inclusion complexes of the type $D{\subset}A_nB_mC_l$ have not been considered, since the included guest does not produce a structural enhancement to the supramolecule.)

[4] a) M. Schmittel, V. Kalsani, *Top. Curr. Chem.* **2005**, *245*, 1–53, and references therein; b) M. Yoshizawa, J. Nakagawa, K. Kumazawa, M. Nagao, M. Kawano, T. Ozeki, M. Fujita, *Angew. Chem.* **2005**, *117*, 1844–1847; *Angew. Chem. Int. Ed.* **2005**, *44*, 1810–1813; c) M. Fujita, N. Fujita, K. Ogura, K. Yamaguchill, *Nature* **1999**, *400*, 52–55; d) C. J. Kuehl, Y. K. Kryschenko, U. Radhakrishnan, S. R. Seidel, S. D. Huang, P. J. Stang, *Proc. Natl. Acad. Sci. USA* **2002**, *99*, 4932–4936; e) B. Olenyuk, J. A. Whiteford, A. Fechtenkr, P. J. Stang, *Nature* **1999**, *398*, 796–799.

[5] By multiple molecular components we mean different molecular components $A_nB_mC_lD_k\ldots Z_x$ and not a large number of the same set of components, that is, A_nB_m. Numerous examples of the latter kind are known.

[6] a) M. C. T. Fyfe, J. F. Stoddart, *Coord. Chem. Rev.* **1999**, *183*, 139–155; b) H. Hofmeier, U. S. Schubert, *Chem. Commun.* **2005**, *19*, 2423–2432.

[7] a) M. Schmittel, A. Ganz, D. Fenske, *Org. Lett.* **2002**, *4*, 2289–2292; b) M. Schmittel, H. Ammon, V. Kalsani, A. Wiegrefe, C. Michel, *Chem. Commun.* **2002**, 2566–2567; c) M. Schmittel, V. Kalsani, A. Wiegrefe, *Chem. Commun.* **2004**, 490–491; d) M. Schmittel, R. S. K. Kishore, *Org. Lett.* **2004**, *6*, 1923–1926; e) V. Kalsani, H. Ammon, F. Jäckel, J. P. Rabe, M. Schmittel, *Chem. Eur. J.* **2004**, *10*, 5481–5492; f) V. Kalsani, H. Bodenstedt, D. Fenske, M. Schmittel, *Eur. J. Inorg. Chem.* **2005**, 1841–1849; g) M. Schmittel, V. Kalsani, J. W. Bats, *Inorg. Chem.* **2005**, *44*, 4115–4117; h) M. Schmittel, V. Kalsani, R. S. K. Kishore, H. Cölfen, J. W. Bats, *J. Am. Chem. Soc.* **2005**, *127*, 11544–11545.

[8] M. Schmittel, A. Ganz, *Chem. Commun.* **1997**, 999–1000.

[9] a) C. A. Hunter, M. N. Meah, J. K. M. Sanders, *J. Am. Chem. Soc.* **1990**, *112*, 5773–5780; b) H. L. Anderson, C. A. Hunter, M. N. Meah, J. K. M. Sanders, *J. Am. Chem. Soc.* **1990**, *112*, 5780–5789; c) S. Yagi, I. Yonekura, M. Awakura, M. Ezoe, T. Takagishi, *Chem. Commun.* **2001**, 557–558; d) S. Yagi, M. Ezoe, I. Yonekura, T. Takagishi, H. Nakazumi, *J. Am. Chem. Soc.* **2003**, *125*, 4068–4069; e) D. M. Guldi, C. Luo, A. Swartz, M. Scheloske, A. Hirsch, *Chem. Commun.* **2001**, 1066–1067; f) D. Jokic, Z. Asfari, J. Weiss, *Org. Lett.* **2002**, *4*, 2129–2132; g) M. Dudic, P. Lhotak, H. Petrickova, I. Stibor, K. Lang, J. Sykora, *Tetrahedron* **2003**, *59*, 2409–2415.

[10] a) H. L. Anderson, *Inorg. Chem.* **1994**, *33*, 972–981; b) P. N. Taylor, H. L. Anderson, *J. Am. Chem. Soc.* **1999**, *121*, 11538–11545; c) T. E. O. Screen, J. R. G. Throne, R. G. Denning, D. G. Bucknail, H. L. Anderson, *J. Am. Chem. Soc.* **2002**, *124*, 9712–9713; d) C. C. Mak, D. Pomeranc, M. Montalti, L. Prodi J. K. M. Sanders, *Chem. Commun.* **1999**, 1083–1084; e) A. L. Kieran, A. D. Bond, A. M. Belenguer, J. K. M. Sanders, *Chem. Commun.* **2003**, 2674–2675; f) N. Bampos, V. Marvaud, J. K. M. Sanders, *Chem. Eur. J.* **1998**, *4*, 335–343; g) C. A. Hunter, R. Tregonning, *Tetrahedron* **2002**, *58*, 691–697; h) L. Baldini, P. Ballester, A. Casnati, R. M. Gomila, C. A. Hunter, F. Sansone, R. Ungaro, *J. Am. Chem. Soc.* **2003**, *125*, 14181–14189; i) M. C. Lensen, S. J. T. van Dingenen, J. A. A. W. Elemans, H. P. Dijkstra, G. P. M. van Klink, G. van Koten, J. W. Gerritsen, S. Speller, R. J. M. Nolte, A. E. Rowan, *Chem. Commun.* **2004**, 762–763.

[11] a) J. Barber, B. Andersson, *Nature* **1994**, *370*, 31–34; b) W. Kühlbrandt, *Nature* **1995**, *374*, 497–498; c) G. McDermott, S. M. Prince, A. A. Freer, A. M. Hawthornthwaite-Lawless, M. Z. Papiz, R. J. Cogdell, N. W. Isaacs, *Nature* **1995**, *374*, 517–521; d) T. Pullerits, V. Sundström, *Acc. Chem. Res.* **1996**, *29*, 381–389.

[12] a) C. K. Chang, I. Abdalmuhdi, *J. Org. Chem.* **1983**, *48*, 5388–5390; b) J. P. Collman, P. S. Wagenknecht, J. E. Hutchinson, *Angew. Chem.* **1994**, *106*, 1620–1639; *Angew. Chem. Int. Ed. Engl.* **1994**, *33*, 1537–1556; c) Y. Deng, C. J. Chang, D. J. Nocera, *J. Am. Chem. Soc.* **2000**, *122*, 410–411.

[13] M. Schmittel, C. Michel, A. Wiegrefe, V. Kalsani, *Synthesis* **2001**, 1561–1567.

[14] T. M. Fasina, J. C. Collings, D. P. Lydon, D. A. Jove, A. S. Batsanov, J. A. K. Howard, P. Nguyen, M. Bruce, A. J. Scott, W. Clegg, S. W. Watt, C. Viney, T. B. Marder, *J. Mater. Chem.* **2004**, *14*, 2395–2404.

[15] Carried out on PC Spartan Pro 1.0.7, Wavefunction Inc., Irvine, CA 92612, USA.

[16] a) L. Flamigni, M. R. Johnston, *New J. Chem.* **2001**, *25*, 1368–1370; b) K. Yamada, H. Imahori, E. Yoshizawa, D. Gosztola, M. R. Wasielewski, Y. Sakata, *Chem. Lett.* **1999**, 235–236.

[17] a) H. Gampp, M. Maeder, C. J. Meyer, A. D. Zuberbühler, *Talanta* **1985**, *32*, 95–101; b) F. J. C. Rossoti, H. S. Rossoti, R. J. Whewell, *J. Inorg. Nucl. Chem.* **1971**, *33*, 2051–2065; c) H. Gampp, M. Maeder, C. J. Meyer, A. D. Zuberbühler, *Talanta* **1985**, *32*, 257–264; d) H. Gampp, M. Maeder, C. J. Meyer, A. D. Zuberbühler, *Talanta* **1986**, *33*, 943–951.

[18] SPECFIT generates multiple fit models. Thus, a 1:1 model was also generated with $\log\beta = 5.9 \pm 0.1$ for **PT·3b** and $\log\beta = 6.4 \pm 0.9$ for **PT·(3b)$_2$**.

[19] a) C. A. Hunter, L. D. Sarson, *Angew. Chem.* **1994**, *106*, 2424–2426; *Angew. Chem. Int. Ed. Engl.* **1994**, *33*, 2313–2316; b) X. Chi, A. J. Guerin, R. A. Haycock, C. A. Hunter, L. D. Sarson, *J. Chem. Soc. Chem. Commun.* **1995**, 2567–2569; c) C. A. Hunter, R. K. Hyde, *Angew. Chem.* **1996**, *108*, 2064–2067; *Angew. Chem. Int. Ed. Engl.* **1996**, *35*, 1936–1939; d) C. A. Hunter, R. J. Shannon, *Chem. Commun.* **1996**, 1361–1362; e) C. C. Mak, N. Bampos, J. M. K. Sanders, *Angew. Chem.* **1998**, *110*, 3169–3172; *Angew. Chem. Int. Ed.* **1998**, *37*, 3020–3023; f) N. Armaroli, F. Diederich, L. Echegoyen, T. Habicher, L. Flamigni, G. Marconi, J.-F. Nierengarten, *New J. Chem.* **1999**, *23*, 77–83.

[20] SPECFIT also generates a 1:1 model with $\log\beta = 5.7 \pm 0.1$ for **PT·3c** and $\log\beta = 9.5 \pm 0.1$ for **PT·(3c)$_2$**, and a 2:2 model with $\log\beta = 16.8 \pm 0.2$ for **(PT)$_2$·(3c)$_2$** and $\log\beta = 9.3 \pm 0.1$ for **PT·(3c)$_2$**.

[21] M. Gardner, A. J. Guerin, C. A. Hunter, U. Michelsen, C. Rotger, *New J. Chem.* **1999**, *23*, 309–316.

[22] T. Timmerman, J.-L. Weidmann, K. A. Jolliffe, L. J. Prins, D. N. Reinhoudt, S. Shinkai, L. Frish, Y Cohen, *J. Chem. Soc. Perkin Trans. 2* **2000**, 2077–2089.

[23] a) M. Holtz, X. Mao, D. Seiferling, A. Sacco, *J. Chem. Phys.* **1996**, *104*, 669–679; b) A. R. Waldeck, P. W. Kuchel, A. J. Lennon, B. E. Chapman, *Prog. Nucl. Magn. Reson. Spectrosc.* **1997**, *30*, 39–68.

[24] a) G. Proni, G. Pescitelli, X. Huang, K. Nakanishi, N. Berova, *J. Am. Chem. Soc.* **2003**, *125*, 12914–12927; b) Z.-Q. Wu, X.-B. Shao, C. Li, J.-L. Hou, K. Wang, X.-K. Jiang, Z.-T. Li, *J. Am. Chem. Soc.* **2005**, *127*, 17460–17468; c) M. Dudič, P. Lhotàk, I. Stibor, H. Petříčkovà, K. Lang, *New J. Chem.* **2004**, *28*, 85–90; d) V. V. Borovkov, J. M. Lintuluoto, M. Sugiura, Y. Inoue, R. Kuroda, *J. Am. Chem. Soc.* **2002**, *124*, 11282–11283; e) V. V. Borovkov, J. M. Lintuluoto, G. A. Hembury, M. Sugiura, R. Arakawa, Y. Inoue, *J. Org. Chem.* **2003**, *68*, 7176–7192; f) J. Brettar, J.-P. Gisselbrecht, M. Gross, N. Solladié, *Chem. Commun.* **2001**, 733–734; g) R. Rein, M. Gross, N. Solladié, *Chem. Commun.* **2004**, 1992–1993.

[25] A. Satake, Y. Kobuke, *Tetrahedron* **2005**, *61*, 13–41.

[26] M. Nappa, J. S. Valentine, *J. Am. Chem. Soc.* **1978**, *100*, 5075–5080.
[27] a) I. Goldberg, *Chem. Eur. J.* **2000**, *6*, 3863– 3870; b) R. K. Kumar, S. Balasubramanian, I. Goldberg, *Inorg. Chem.* **1998**, *37*, 541–552.
[28] G. J. Kubas, *Inorg. Synth.* **1979**, *19*, 90–92.
[29] a) M. Maeder, A. D. Zuberbühler, *Anal. Chem.* **1990**, *62*, 2220–2224; b) H. Gampp, M. C. J. Maeder, A. D. Zuberbühler, *Talanta* **1986**, *33*, 943–951.

Received: April 3, 2006
Published online: July 24, 2006

